Earth and Planetary Science Letters 384 (2013) 154–164

Contents lists available at ScienceDirect

Earth and Planetary Science Letters

www.elsevier.com/locate/epsl

Did rock avalanche deposits modulate the late Holocene advance of Tiedemann Glacier, southern Coast Mountains, British Columbia, Canada?

Brian Menounos [a,*], John J. Clague [b], Garry K.C. Clarke [c], Shaun A. Marcott [d], Gerald Osborn [e], Peter U. Clark [d], Christina Tennant [a], Anthony M. Novak [d]

[a] Geography Program and Natural Resources and Environmental Studies Institute, University of Northern British Columbia, 3333 University Way, Prince George, BC, V2N 4Z9, Canada
[b] Department of Earth Sciences, Simon Fraser University, 8888 University Drive, Burnaby, BC, V5A 1S6, Canada
[c] Department of Earth, Ocean and Atmospheric Sciences, University of British Columbia, 2207 Main Mall, Vancouver, BC, V6T 1Z4, Canada
[d] College of Earth, Ocean, and Atmospheric Sciences, 104 COAS Admin Bldg., Corvallis, OR 97331, USA
[e] Department of Geosciences, University of Calgary, 844 Campus Place Northwest, Calgary, AB, T2N 1N4, Canada

ARTICLE INFO

Article history:
Received 22 February 2013
Received in revised form 26 September 2013
Accepted 4 October 2013
Available online xxxx
Editor: J. Lynch-Stieglitz

Keywords:
Holocene glacier fluctuations
surface exposure dating
numerical modeling
debris-covered glacier
rock avalanche

ABSTRACT

Most glaciers in western North America with reliable age control achieved their maximum Holocene extents during final advances of the Little Ice Age. Tiedemann Glacier, a large alpine glacier in western Canada, is an enigma because the glacier constructed lateral moraines that are up to 90 m higher, and extend 1.8 km farther downvalley, than those constructed during the Little Ice Age. Our data show that the activity of the glacier is more complex than originally documented and that the glacier advanced many times during the past six thousand years. Surface exposure dating and radiocarbon ages of stumps beneath till demonstrate that the glacier achieved its maximum Holocene extent at about 2.7 ka. We hypothesize that one or more rock avalanches delivered surface debris to the glacier and caused the 2.7 ka glacier advance to be much larger than can be explained by climate forcing. To test our hypothesis, we developed and used a surface debris advection routine coupled to an ice dynamics model. Our results show that even a moderately sized rock avalanche (10×10^6 m^3) delivered to the top of the ablation zone could cause the glacier to thicken and advance far beyond its Little Ice Age limit.

1. Introduction

With few exceptions, glaciers in western North America achieved their maximum Holocene extents during the final centuries of the Little Ice Age. Many moraines that lie outside Little Ice Age limits, initially believed to be Holocene landforms, are now known to be latest Pleistocene in age (Osborn and Luckman, 1988; Davis et al., 2009). Denton and Karlén (1977) documented several mid-to-late Holocene (Neoglacial) terminal moraines in the Saint Elias Mountains in Yukon Territory that extend beyond Little Ice Age deposits, but these glaciers surge or have unusually thick debris cover that complicates the relation between climate and glacier response (Denton and Karlén, 1977; Yde and Paasche, 2010).

Porter and Denton (1967) first described regional evidence for an advance of North American alpine glaciers about 2700 years ago. Tiedemann Glacier, located in the southern Coast Mountains of British Columbia, advanced well beyond its Little Ice Age limit during this regional advance. In particular, the stratigraphic and geomorphic evidence for the late Holocene 'Tiedemann Advance' at its type locality is compelling. Lateral moraines associated with this advance occur along the lower 12 km of the ablation zone of the glacier, rise up to 90 m above the Little Ice Age moraine crest, and extend 1.8 km downvalley from the outermost Little Ice Age terminal moraine. Glacier downwasting during the 20th century exposed lateral moraines composed of multiple tills, glaciofluvial sediments, and subfossil wood. Fulton (1971) obtained radiocarbon ages on bulk samples of organic sediments just above and below a thin layer of outwash in a bog just outside the Tiedemann north lateral moraine. These ages constrain the age of the Tiedemann Advance to 2.16–3.33 ka (2σ range) (kilo calendar yrs BP). Arsenault et al. (2007) narrowed this age range to 2.18–2.75 ka based on radiocarbon ages on conifer needles from the lower and upper contact of the outwash. Radiocarbon ages from wood in the north Tiedemann lateral moraine suggest that the Tiedemann Advance began about 3.30 ka and that the glacier remained in an advanced position until 1.90 ka, after which it retreated (Ryder and Thomson, 1986).

* Corresponding author.
E-mail address: menounos@unbc.ca (B. Menounos).

0012-821X/$ – see front matter
http://dx.doi.org/10.1016/j.epsl.2013.10.008

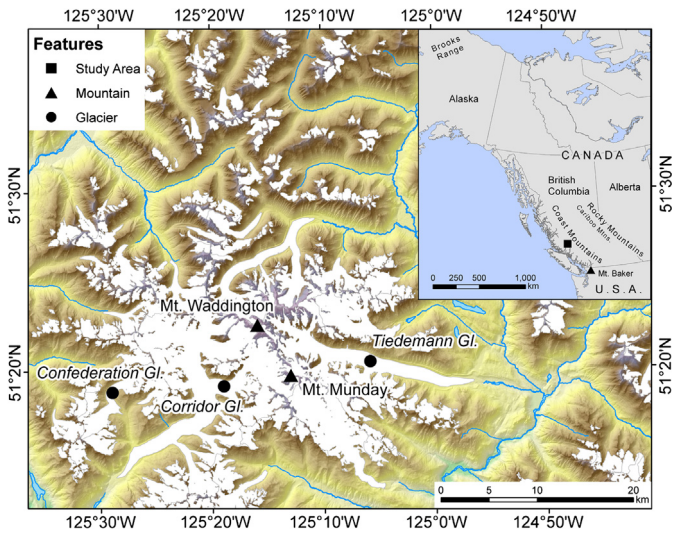

Fig. 1. Color shaded relief map of the study area.

Given the unusual behavior of Tiedemann Glacier during the middle Neoglacial, we reexamined the stratigraphy and moraine record of the glacier. Our motivation was two-fold. First, we sought to obtain additional stratigraphic and chronological information that might reveal additional details about the behavior of Tiedemann Glacier during the period 3.3–1.9 ka. Continued mass wasting of the lateral moraines and thinning of the glacier by several tens of meters since Ryder and Thomson (1986) visited the glacier in 1977 and 1978 offered the possibility that we could examine new stratigraphic sections. Second, we wished to verify the age of the outermost moraines at Tiedemann Glacier because it is one of only a few sites in western Canada where Holocene moraines lie outside Little Ice Age moraines.

In this paper, we present new stratigraphic and chronologic evidence for the timing of fluctuations of the Tiedemann Glacier between 5.89 ka and 0.32 ka and offer an explanation for its idiosyncratic behavior. We first describe the study area and the methods used to temporally constrain the activity of the glacier. We then describe the stratigraphy of the north lateral moraine and present surface exposure ages that confirm the age of the Tiedemann Advance. Finally, we use a coupled ice dynamics and surface debris advection model to investigate the possibility that surface debris cover may explain the unusual behavior of the glacier.

2. Study area and methods

Tiedemann Glacier (Figs. 1 and 2) flows 23 km east from Mount Waddington (4019 m asl) to its terminus at 360 meters above sea level (m asl). The lower 17 km of the glacier, which lies in the ablation zone, has a width of 1–1.5 km. The net mass balance of Tiedemann Glacier was strongly negative during the latter half of the 20th century — the glacier thinned, on average, 25 m and lost 1.67 ± 0.17 km^3 of ice (water equivalent) over the period 1949–2009 (Tennant et al., 2012). In 2005, debris covered about 27% of the glacier surface, primarily its lowest 8.5 km. Sequential aerial photographs indicate that this debris cover increased in extent as the glacier thinned over the past 60 years.

The upper portion of the glacier is bordered by steep slopes with relief up to 1000 m, whereas the lower part and its associated Neoglacial moraines extend across an area of subdued relief (Figs. 1 and 2). The Little Ice Age moraine, termed the "inner moraine" by Ryder and Thomson (1986), is a prominent single- or multiple-crested ridge that reaches up to 100 m above the glacier surface and impounds two lakes (Fig. 2). The maximum Holocene extent of the glacier is delineated by a conspicuous blocky lateral moraine,

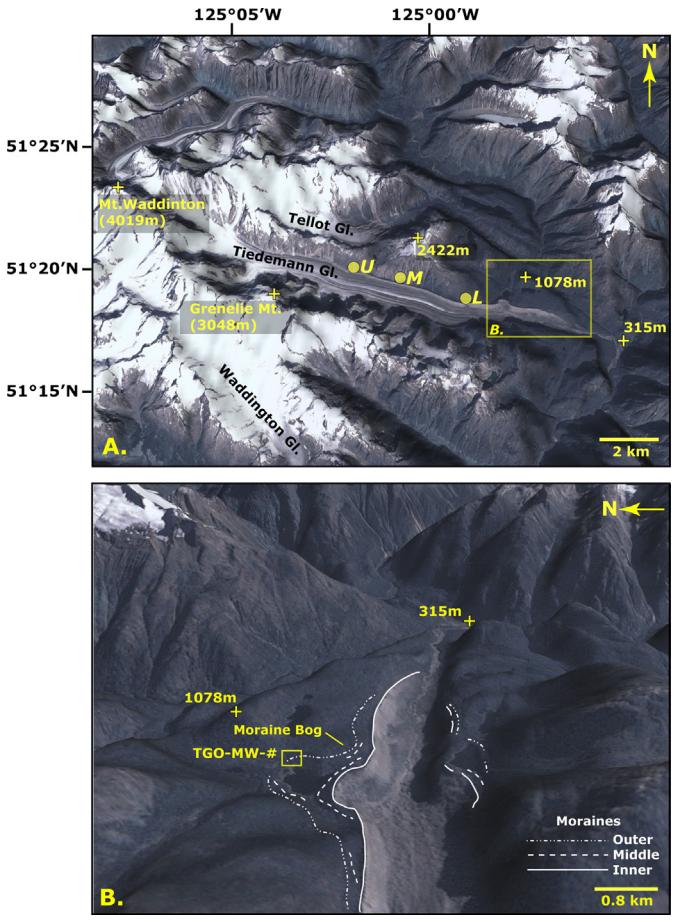

Fig. 2. Oblique aerial photograph overlain with Landsat7 imagery of the southern Coast Mountains near Mount Waddington and Tiedemann Glacier. The yellow box indicates the area from which blocks were collected for surface exposure dating. The relief is vertically exaggerated 1.5 times to improve clarity (distance scale is approximate). Image generated with NASA World Wind 1.4. Labels U, M, and L, respectively, denote "upper", "middle", and "lower" stratigraphic sections. "TGO-MW" denotes the sampling site for surface exposure ages. (For interpretation of the references to color in this figure, the reader is referred to the web version of this article.)

the "outer moraine" of Ryder and Thomson (1986). The outer lateral moraine on the north side of the glacier is continuous over a distance of almost 10 km. A correlative moraine is present along the south side of the glacier, but it is poorly preserved and is only continuous over a distance of less than 4 km. About 3 km above the terminus, on the north side of the glacier, the "outer moraine" comprises three separate ridges (Fig. 2). Mature forest and a well-developed soil on these ridges contrast with the sparse vegetation and lack of soil development on the "inner moraine," suggesting a significant difference in the age of the features.

2.1. Lateral moraine stratigraphy

We documented the stratigraphy of the north lateral moraine of Tiedemann Glacier at three sites during the summers of 2005 and 2006. Exposed sediment sections were steep, difficult to access, and subject to rockfall. For safety reasons, our stratigraphic work thus focused on determining the general sediment character and broad stratigraphic relationships exposed in the north lateral moraine.

A hand-held GPS was used to record section locations. We determined relative elevations with a barometric altimeter and tied readings to several base stations at the edge of the glacier. The absolute elevations of the base stations were determined from a

digital elevation model (DEM) produced from data provided by the Province of British Columbia (British Columbia Ministry of Environment, Land and Parks, 1992). We also checked elevations of our sections using aerial-triangulated, stereo photogrammetric models with a nominal ground sampling distance of 50 cm and vertical errors of less than 2 m.

2.2. Surface exposure dating

We sampled blocks from the north lateral of the type-Tiedemann moraine for ^{10}Be surface exposure dating (Fig. 2). To limit the possibility of complex boulder exposure histories (e.g. prior exhumation, burial, boulder toppling), we selected relatively flat-surfaced, unweathered blocks that were 1 m or more in height and located on stabilized portions of the moraine crest. One to three kilograms of rock was sampled from the top 2–4 cm of each boulder for cosmogenic chemistry. We made shielding and surface slope measurements in the field using a Suunto clinometer and Brunton compass, respectively. We also photographed each boulder and documented its geometry.

We prepared beryllium targets at Oregon State University following the methods of Licciardi (2000) and Rinterknecht (2004), with the modifications of Goehring (2006). ^{10}Be/^{9}Be ratios were measured at Purdue University in the Purdue Rare Isotope Measurement (PRIME) Laboratory and referenced relative to the revised ICN standard (Nishiizumi et al., 2007). After correcting for the system blank, we converted ^{10}Be/^{9}Be ratios to ^{10}Be atoms per gram of quartz (Table 1), from which we calculated ages using the CRONUS-Earth online calculator (v.2.2) (Balco et al., 2008) and the northeastern North America production rate (Balco et al., 2009).

Given the potential for individual ^{10}Be ages to contain young and old outliers, we use the median and interquartile range as metrics of central tendency and dispersion. We also report the median age of our ^{10}Be ages in kilo calendar years (AD 1950 = 0.0 ka) to facilitate comparison to reported radiocarbon ages.

2.3. Radiocarbon dating

We submitted 12 subfossil wood samples for radiocarbon dating by conventional (radiometric) and accelerator mass spectrometry (AMS) methods at Beta Analytic Ltd. and Keck Carbon Cycle AMS Laboratory (University of California Irvine). We calibrated radiocarbon ages using the program CALIB 5.0.2 (Stuiver et al., 2005). All wood ages are reported as calibrated, kilo year (ka) age ranges [$\pm 2\sigma$].

2.4. Ice dynamics model

To investigate the role that debris cover may have played in past fluctuations of Tiedemann Glacier, we coupled an ice dynamics model with horizontal advection of debris introduced to the glacier surface. Christian Schoof (University of British Columbia) developed the vertically integrated ice dynamics model based on the shallow ice approximation. In contrast to the treatments of Plummer and Phillips (2003) and Kessler et al. (2006), we employ a semi-implicit, finite difference scheme (e.g., Le Meur and Vincent, 2003) and, optionally, apply "super-implicit" time-stepping (Hindmarsh, 2001, p. 240) and flux limiters (Jarosch et al., 2012b).

The ice dynamics model solves mass conservation and vertically integrated momentum equations on a rectangular grid. We assumed the ice to be isothermal and at 0 °C, and thus neglect thermal energy. The governing equation for the change of ice thickness over time is

$$\frac{\partial h}{\partial t} = \dot{B} - \nabla_{xy} \cdot \mathbf{q} \qquad (1)$$

Table 1
Radiocarbon ages.

Laboratory No.[a]	Site	Location (lat. ° N, long. ° W)	Context	Elevation (m asl)	Radiocarbon age (^{14}C ka)[b]	Calibrated age (ka)[c]	Reference
Beta-220942	Upper	51.3434, 125.0704	Detrital root or branch	1355	210 ± 50	0.00–0.43	This study
UCIAMS-40664	Upper	51.3434, 125.0704	Detrital tree stem	1350	375 ± 20	0.50–0.33	This study
Beta-220939	Middle	51.3377, 125.0385	In situ tree stem near top of unit 6	1150	2710 ± 40	2.92–2.75	This study
UCIAMS-40662	Middle	51.3377, 125.0385	In situ tree stem near top of unit 6	1150	2820 ± 15	2.96–2.87	This study
Beta-220940	Middle	51.3377, 125.0385	In situ tree stem in wood mat (unit 4)	1135	3760 ± 60	4.38–3.93	This study
UCIAMS-40663	Middle	51.3377, 125.0385	Detrital tree stem in wood mat (unit 4)	1135	3865 ± 20	4.41–4.18	This study
Beta-220941	Middle	51.3274, 124.9763	Wood fragments in silt and sand (unit 2)	1125	5010 ± 40	5.89–5.65	This study
Beta-220938	Lower	51.3274, 124.9763	In situ tree stem	945	2520 ± 50	2.75–2.37	This study
Beta-220937	Lower	51.3274, 124.9763	In situ tree stem in silt	940	2670 ± 50	2.87–2.73	This study
UCIAMS-40661	Lower	51.3274, 124.9763	Detrital tree stem in wood mat	935	2935± 15	3.20–3.00	This study
Beta-220936	Lower	51.3274, 124.9763	In situ tree stem in silt	935	3690 ± 50	4.22–3.89	This study
UCIAMS-40660	Lower	51.3274, 124.9763	Twig in silt	935	3820 ± 20	4.29–4.10	This study
S-1474	Site 1 (upper)	51.3347, 125.0708	Detrital log in uppermost till	1360	300 ± 60	0.50–0.00	Ryder and Thomson (1986)
S-1473	Site 1 (upper)	51.3347, 125.0708	Detrital log in sand unit ca. 12.5 m below moraine crest	1360	1330 ± 65	1.35–1.08	Ryder and Thomson (1986)
S-1472	Site 2 (lower)	51.3278, 124.9750	Detrital log at contact between lower sand unit and uppermost till	1015	65 ± 100	0.29–0.00	Ryder and Thomson (1986)
S-1471	Site 2 (lower)	51.3278, 124.9750	Log in wood mat	990	2355 ± 60	2.70–2.16	Ryder and Thomson (1986)
S-1470	Site 2 (lower)	51.3278, 124.9750	Wood fragment from paleosol	980	3345 ± 115	3.88–3.36	Ryder and Thomson (1986)
TO-10756	Bog	51.3300, 125.9283	Macrofossils directly below silt bed	890	2530 ± 50	2.75–2.37	Arsenault et al. (2007)
TO-10755	Bog	51.3300, 125.9283	Macrofossils directly above silt bed	890	2290 ± 50	2.43–2.15	Arsenault et al. (2007)

[a] Radiocarbon laboratory: Beta = Beta Analytic Inc; S = University of Saskatchewan; UCIAMS = University of California; TO = University of Toronto.
[b] In situ and detrital tree stem ages determined on outer rings. Position of dated rings in logs dated by Ryder and Thomson (1986) are unknown.
[c] Calendar ages ($\pm 2\sigma$) determined using CALIB 5.02 (Stuiver et al., 2005).

where $h = h(x, y, t)$ is ice thickness, $\dot{B} = \dot{B}(x, y, t)$ represents the net mass balance rate of ice at the glacier surface, ∇_{xy} is the two-dimensional gradient operator, and $\mathbf{q} = q_x(x, y, t)\mathbf{i} + q_y(x, y, t)\mathbf{j}$ is the two-dimensional ice flux vector where

$$\mathbf{q} = -\frac{2A(\rho g)^n |\nabla_{xy} S|^{n-1}}{n+2} h^{n+2} \nabla_{xy} S + \mathbf{v}_B h \quad (2)$$

In Eq. (2), $A = 7.5738 \times 10^{-17}$ Pa^{-3} a^{-1} is the coefficient and $n = 3$ is the exponent of Glen's flow law for ice creep, $\rho = 910$ kg m^{-3} is the ice density, g $= 9.81$ m s^{-2} is the gravity acceleration, S is the ice surface elevation, and $\mathbf{v}_B = u_B\mathbf{i} + v_B\mathbf{j}$ is the basal sliding velocity vector.

Distributed mass balance ($\dot{B}$) was determined through temperature downscaling and the use of an orographic precipitation model (Jarosch et al., 2012a). We used climate fields for the period 1979–2005 to generate an epoch-averaged $\dot{B}$ that simulates climatic conditions less favorable for ice growth than those of Neoglacial time. We estimated subglacial topography beneath Tiedemann Glacier using an inversion method described in Clarke et al. (2013). We ran the model at 200 m resolution, which is suitably detailed to resolve the topographic complexities of the region. The model was initialized with zero ice cover, and glaciers were allowed to evolve under the prescribed mass balance forcing. We ran the model for 1000 years to ensure that steady-state conditions were achieved. To simplify our experiments, we did not allow sliding at the glacier bed because we lack empirical data such as water pressure or the presence of a deformable till layer beneath the glacier. Both factors, including detailed measurements of surface velocity, are required to choose an appropriate sliding law. We emphasize that our modeling exercise was performed simply to test the plausibility that the glacier could advance following the sudden input of debris.

2.5. Debris advection model

To examine the role that landslide debris might have on glacier behavior, we coupled our ice dynamics model to a surface debris transport model. Our model conserves debris volume through time, but it differs from the approach used by Vacco et al. (2010), which only models the down-glacier (1-D) movement of debris. Because our ice dynamics model does not track vertical changes in ice speed, it only applies to surface debris transport below the equilibrium line. Debris movement is directly coupled to surface ice flow; debris thickness for a given model time step is

$$\frac{\partial h_\sigma}{\partial t} = -u_S \frac{\partial h_\sigma}{\partial x} - v_S \frac{\partial h_\sigma}{\partial y} \quad (3)$$

where $h_\sigma = h_\sigma(x, y, t)$ is debris thickness, and u_S and v_S are x and y components of the ice surface velocity vector $\mathbf{v}_S = u_S\mathbf{i} + v_S\mathbf{j}$. Eq. (3) is a hyperbolic partial differential equation, known as the advection equation, which we numerically solve using standard Riemann methods (LeVeque, 2002).

We ran the coupled glaciation-debris transport model for different debris thicknesses (volumes) and elevations at which the debris was introduced to the surface of the glacier. We used the equilibrium state that glaciers achieved with $\dot{B}$ after 1000 years to define our initial conditions, after which we instantaneously added debris sheets ranging from 0.5 m to 5.0 m thick at different 100-m elevation zones in the ablation area of the glacier. We added the debris mass to the total mass of the ice column to calculate the driving stress for ice flux. Each of our 110 simulations took about two hours on a computer (single thread on a 2.4 GHz Intel Xeon quad core CPU).

At time scales of a decade or more, the primary mechanism by which surface debris could affect changes in glacier length is by reducing surface melt. We modified the melt rate under debris using averaged empirical values reported by Nicholson and Benn (2006). For debris of thickness $h_\sigma > 0.05$ m, $\dot{B}$ was reduced according to

$$\dot{B}(h_\sigma) = 0.0856\dot{B}(0)h_\sigma^{-0.837} \quad (4)$$

For a mass balance rate of -10 m a^{-1}, for example, Eq. (4) reduces $\dot{B}$ to -1.5, -0.5, and -0.2 m a^{-1}, where h_σ equals 1.0, 2.0, and 5.0 m, respectively.

3. Results

3.1. North lateral moraine stratigraphy

Sediments are exposed nearly continuously over a distance of 12 km in the northern inner (Little Ice Age) lateral moraine of Tiedemann Glacier. We documented the stratigraphy at three sites ("upper," "middle," and "lower sites" in Figs. 2 and 3) and confirmed continuity and correlation of units during helicopter transverses along the length of the moraine. The upper and lower sites are near sites 1 and 2, respectively, of Ryder and Thomson (1986). The middle site is about midway between them. Below, we describe the stratigraphy at the middle site, where all of the units that we recognize are present and where many of our radiocarbon ages were obtained.

The middle site is 6.8 km upvalley from the 2005 glacier terminus and approximately 9.8 km down-glacier from the equilibrium line (Fig. 3). The section is about 100 m high, of which the lowest 35 m is covered by colluvium down to the glacier margin at about 1125 m asl. The exposed sediments comprise several similar diamicton units separated by generally thin units of sand, wood mats, or paleosols (Fig. 3). All diamicton units are massive to weakly stratified, olive-grey in color, and contain subrounded to angular clasts up to boulder size. Many of the clasts are striated and faceted. We identified nine units; from the base of the exposure to the top, they are: (1) matrix-supported diamicton (>1 m thick); (2) oxidized silt and sand with detrital wood fragments (this unit is discontinuous and <1 m thick); (3) clast-supported diamicton (ca. 8 m thick); (4) wood mat with detrital tree stems and branches and stumps in growth position (<1 m thick); (5) clast-supported diamicton (11 m thick); (6) horizontally stratified, fine-to-coarse sand with some cross-beds indicating flow in a down-glacier direction (4 m thick); vertical and tilted stems of trees are rooted in the upper part of the unit and extend into the overlying diamicton; the unit pinches out along the moraine between units 5 and 7; oxidized sediment occurs at the contacts between units 6 and 7, and between units 5 and 7 where unit 6 is absent; (7) clast-supported diamicton (13 m thick); a thin light-colored zone separates this unit from the overlying diamicton; (8) olive-grey, rubbly to blocky, clast-supported diamicton (12 m thick); the uppermost sediment in the unit is oxidized and contains some logs and branches; (9) clast-supported diamicton similar to, but not as coarse as, unit 8 (5 m thick); the unit forms the crest of moraine, which has an elevation of about 1225 m at this site. Contacts between adjacent units are sharp. Notably, the contact between units 7 and 8 can be traced for several kilometers up-glacier and down-glacier from the middle section. Clasts in the diamicton forming units 7 and 8 are notably angular.

A fragment of wood recovered from unit 2 yielded an age of 5.89–5.65 ka (Fig. 3, Table 1). Two outer-ring radiocarbon ages were obtained on wood recovered from unit 4. A stump yielded an age of 4.38–3.93 ka, and a detrital tree stem from this unit gave an age of 4.41-4.18 ka.

Two outer-ring radiocarbon ages also were obtained from unit 6. A 30-cm-diameter, 2-m-high vertical stem rooted near the top of unit 6 returned an age of 2.96–2.87 ka, and a rooted stem inclined down-glacier yielded an age of 2.92–2.75 ka (Table 1). We obtained five radiocarbon ages from the same unit at the lower

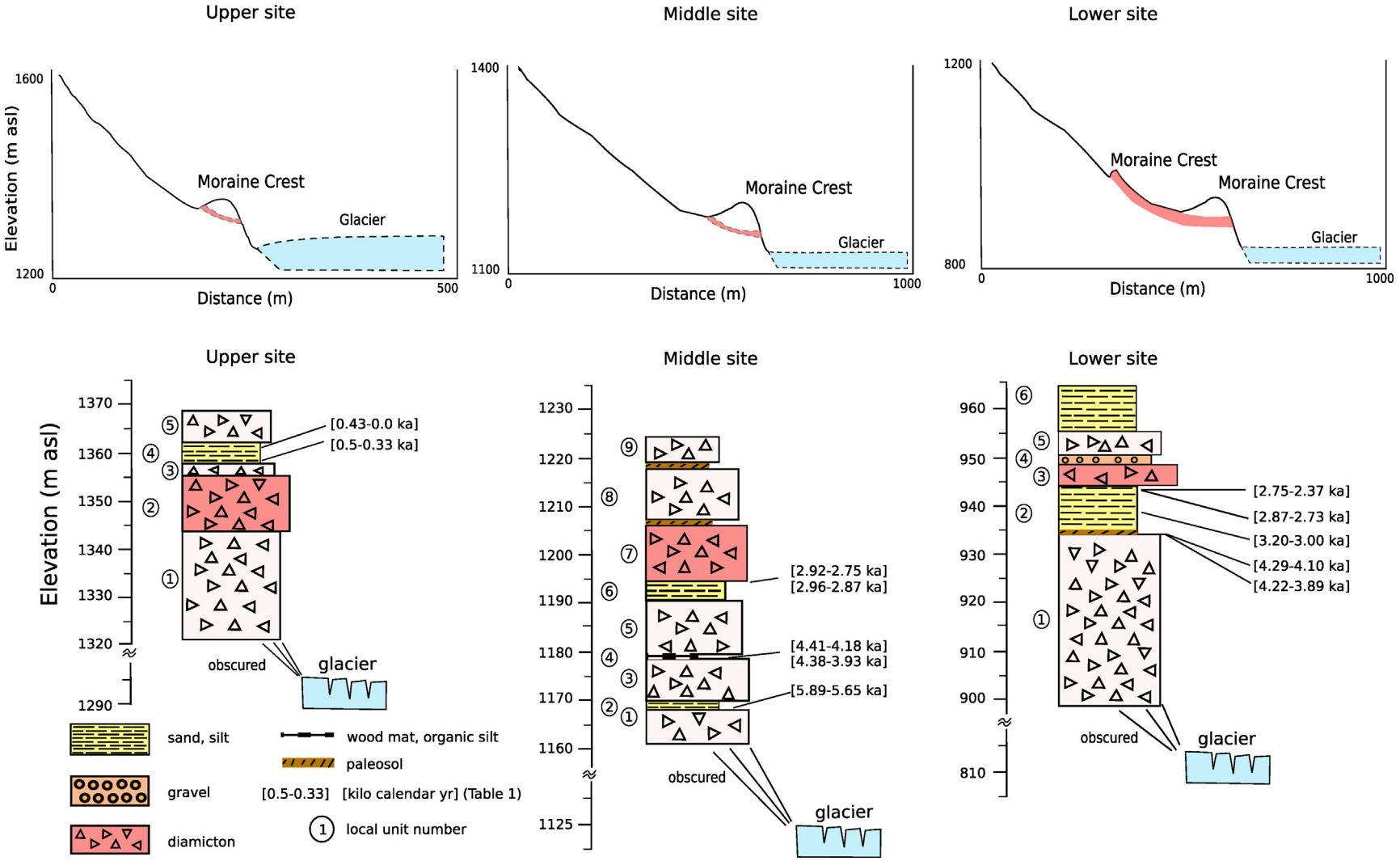

Fig. 3. Top: Cross-valley profiles through the north lateral moraine of Tiedemann Glacier at the upper, middle, and lower sites. The lateral moraine of the Tiedemann Advance lies above the Little Ice Age moraine at the lower site, at about the same elevation as the LIA moraine at the middle site, and beneath the LIA moraine at the upper site. Bottom: Measured stratigraphic sections at the upper, middle, and lower sites. Elevations of the glacier surface based on measurements made on aerial photographs taken in 2005. Shaded (red) diamicton (units 2, 7, and 3 of upper, middle, and lower sites, respectively) is associated with the Tiedemann Advance. Variable widths represent relative resistance to erosion of the units. (For interpretation of the references to color in this figure, the reader is referred to the web version of this article.)

site. There the unit contains vertical stems and roots of in situ trees at four stratigraphic levels. The stems and roots are associated with thin layers of organic-rich silt and peat. Outer rings of a 0.3-m-diameter vertical tree stem associated with a 1–2-cm-thick organic silt layer at the base of the unit returned an age of 4.22–3.89 ka. A twig with delicate branches recovered from the organic silt bed in which this dated tree stem is rooted yielded an age of 4.29–4.10 ka. A peaty wood mat 3 m higher contains tree roots and detrital logs; the outer rings of one of the logs returned an age of 3.20–3.00 ka. Another 3 m higher is another rooting surface with in situ stems of trees up to 70 cm in diameter. A dated stem with about 70 rings and adventitious roots about 10 cm above the lowest rooting horizon yielded an age of 2.87–2.73 ka. Finally, a 3-m-high vertical stem rooted near the top of the unit and extending up into the overlying diamicton returned an age of 2.75–2.37 ka.

The uppermost diamicton (unit 9) can be traced up-glacier to the upper study site. There it overlies sand that contains detrital wood from which we obtained two radiocarbon ages. The outer rings of a 3-m-long detrital tree stem, about 10 cm in diameter, yielded a calibrated age of 0.33–0.50 ka, and a detrital root or branch gave an age of 0.43–0 ka.

3.2. Stratigraphic interpretation

We interpret diamicton units at our three study sites to be till deposited by Tiedemann Glacier at its north lateral margin. The striated clasts in the diamictons and the poor sorting and weak to non-existent stratification argue for a glacial origin. Furthermore, the uppermost diamicton is associated with the LIA moraine, which is obviously glacial. The only possible alternative origin, avalanching from the north wall of the valley, can be ruled out at the middle and lower sites based on the following arguments. Because of similarities in age, the Tiedemann-age diamicton at the lower site is associated with the lateral moraine that lies 90 m above the LIA lateral moraine on the adjacent valley wall (Fig. 3). This relation precludes an avalanche origin for both the Tiedemann and LIA diamictons at the lower site. The Tiedemann moraine at the middle site lies at about the same elevation as the LIA moraine. The Tiedemann-age diamicton at this site is too high and too distant from the north valley wall to have been emplaced by avalanches. This argument also requires that the overlying diamictons, which we interpret to date to the LIA, are glacial in origin.

An avalanche origin for the lowest (pre-Tiedemann) diamicton units at the middle study site cannot be ruled out based on the arguments above. Given their similarities to the Tiedemann and LIA diamictons, however, we conclude that a glacial origin is more likely than an avalanche origin.

The conspicuous sand units at the middle and lower sites are ice-marginal outwash. These units correlate, although deposition of sand at the lower site was separated by intervals of stability and forest growth spanning at least several decades and possibly up to a few centuries. Till was being deposited at the middle site by approximately 4 ka, when the first sand was accumulating at the lower site. The sand unit at the middle site was deposited at the margin of Tiedemann Glacier during the Tiedemann Advance. Sand deposition at that site ended when Tiedemann Glacier thickened and overrode unit 6.

The presence of four rooting horizons within the Tiedemann-age sand unit at the lower site argues for decadal- or centennial-scale fluctuations of Tiedemann Glacier. Each of the four layers records a period of stability lasting at least several decades, separated by periods of deposition of sandy outwash at the margin of the glacier. Each period of outwash deposition indicates some thickening of Tiedemann Glacier at the lower site.

3.3. Surface exposure ages

Based on different scaling models, the median cosmogenic ^{10}Be ages range from 2.69 $\pm$ 0.54 to 2.72 $\pm$ 0.52 ka (Table 2). The range in ages arises from differences in the scaling function applied in each of the methods and how that scaling relates to the site-specific production rates through time (Balco et al., 2008). Our dataset contains one outlier (TGO-MW-07), which has an age that is nearly 25 times older than the mean age of the other blocks. The sample is therefore assumed to have inherited ^{10}Be atoms from a prior exposure history. If we exclude this sample, the median age is reduced by less than 1% and the interquartile range is reduced by a factor of about 3.5. The refined 2σ ^{10}Be age range for the outermost Tiedemann moraine is 2.93–2.39 ka.

If the blocks at our field site experienced significant snow cover, an added correction is needed to account for the additional shielding of the blocks from cosmogenic exposure. Assuming a simple snow burial history where the blocks were covered by 100 cm of snow with a density of 0.3 g cm^{-3} for four months of the year, an average correction of 140 years would be needed. The true snow history cannot be determined, but this additional correction is likely a maximum value and within our age uncertainty. Therefore, it is not applied to our block ages and simply noted here. In addition, we did not correct for surface erosion because of the short exposure history of the blocks.

3.4. Debris modeling results

When driven with 1979–2005 surface mass balance fields ($\dot{B}$), Tiedemann Glacier achieves a steady-state extent during the Tiedemann Advance that is only slightly smaller than it achieved during the Little Ice Age (upper left panel of Fig. 4). A debris cover, however, changes the response of the glacier. As an example, we show the glacier response to the sudden input of a sheet of debris with a volume of 10×10^6 m^3 and a thickness of 4 m near the top the ablation zone of the glacier (Fig. 4). The debris moves more than 10 km down-glacier within decades. The glacier does not begin to advance, however, for another 30 years and achieves its maximum downvalley extent after about 200 years. Thereafter, the extended terminus thins and decays (Fig. 4).

Changes in ice thickness from equilibrium conditions through time clearly show the build-up and decay of ice that preferentially occurs at lower elevations (Fig. 5). Thickness changes greater than 50 m occur for much of the ablation zone below 1200 m asl (Fig. 5). Thickness-change curves for different elevation bands reveal that the ice that builds up beneath the debris cover moves down-glacier as a kinematic wave, similar to what has been observed for glaciers mostly free of surface debris (Meier, 1962).

We determined from our 110 simulations that the largest changes in glacier length from steady-state conditions occurred when a large amount of debris was introduced directly below the equilibrium line of Tiedemann Glacier. The changes are large, however, even with moderate volumes of debris when it is evenly distributed across the uppermost zone of the ablation area (Fig. 6).

4. Discussion

4.1. Holocene activity of Tiedemann Glacier

The history of Tiedemann Glacier is more complex than originally reported by Ryder and Thomson (1986). Our data suggest that the glacier advanced many times during the past 6000 years and that even during the Tiedemann Advance (2.75–2.18 ka), it fluctuated markedly on decadal and centennial timescales. If the detrital wood sample below the lowest unit of till at the middle site along the north lateral moraine is associated with

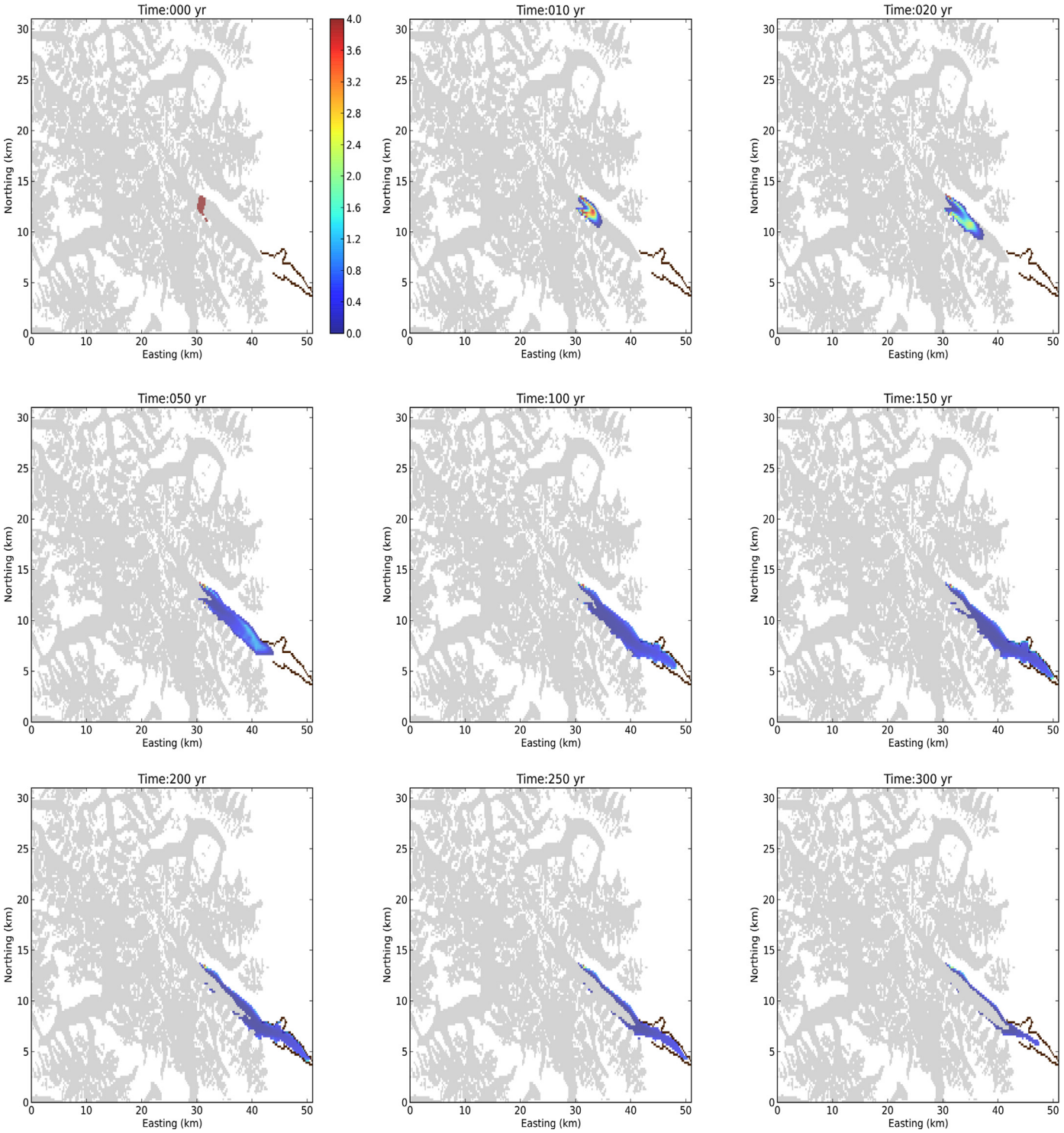

Fig. 4. Response of Tiedemann Glacier to instantaneously adding 10×10^6 m^3 of surface debris of uniform thickness (4 m) near the top the ablation zone of the glacier (1600–1700 m asl). The upper left panel shows the initial surface area of the glacier at the start of the experiment (brown line delimits outermost moraine). Color bar denotes debris thicknesses in meters (debris less than 1 cm is not shown). (For interpretation of the references to color in this figure, the reader is referred to the web version of this article.)

Table 2
Surface exposure ages.

Sample No.	Latitude (° N)	Longitude (° W)	Elevation (m asl)	Density (g cm^{-3})	Thickness (cm)	Shielding correction	Weight (g quartz)	^{10}Be (10^3 at g^{-1})	^{10}Be error (10^3 at g^{-1})
TGO-MW-01	51.337	124.931	790	2.65	2	0.99	36.018	22.23	1.98
TGO-MW-02	51.337	124.931	790	2.65	2	0.99	41.294	26.46	2.12
TGO-MW-03	51.337	124.931	790	2.65	2	0.99	28.338	19.65	2.13
TGO-MW-07	51.337	124.931	790	2.65	2	0.99	20.478	541.50	267.11
TGO-MW-08	51.337	124.932	780	2.65	2	0.97	37.279	21.32	6.40
TGO-MW-09	51.337	124.932	780	2.65	2	0.97	37.902	20.60	2.43

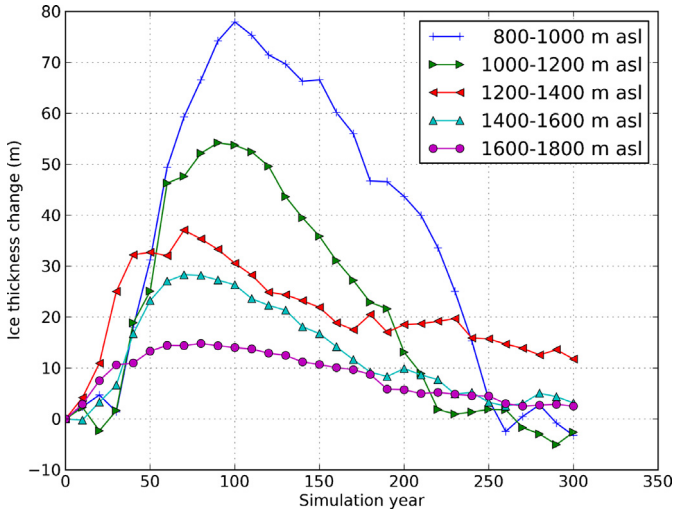

Fig. 5. Ice thickness changes through time.

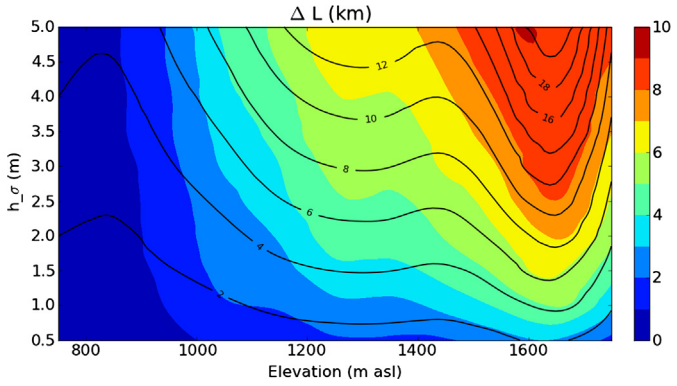

Fig. 6. Changes in the length of Tiedemann Glacier based on debris sheets of differing thicknesses (h_σ [m]) introduced to 100 m elevation zones of the glacier below the equilibrium line altitude. Colors denote changes in glacier length (km). Solid black contours define the associated debris volumes (10^6 m^3) of the 110 experiments for a given debris thickness. (For interpretation of the references to color in this figure, the reader is referred to the web version of this article.)

glacier expansion, Tiedemann Glacier commenced an advance soon after 5.89–5.65 ka. This age is similar to the age of detrital wood (5.75–5.49 ka) found within till at Confederation Glacier (Coulthard et al., 2013), which flows from the southwest flank of Mount Waddington (Fig. 1). Both of these ages overlap the range (7.50–5.00 ka) for widespread early Neoglacial glacier expansion elsewhere in the Coast Mountains (Menounos et al., 2009) and are consistent with Northern Hemisphere cooling beginning around 6.5 ka (Marcott et al., 2013).

The glacier advanced again after 4.38–3.89 ka, based on the 2σ age range of two radiocarbon ages on stumps in growth position below till (Table 1). These ages are supplemented by several ages on detrital wood obtained in this study and by Ryder and Thomson (1986) (Table 1). Based on the ages of four stumps in growth position below till (Table 1), Tiedemann Glacier advanced again after 2.96–2.37 ka. This large age range arises from a prominent plateau in the radiocarbon calibration curve at this time. All five scaling methods used for the ^{10}Be samples yielded ages for the outer moraine that are similar to the radiocarbon ages on stumps in growth position directly below till associated with the construction of the north lateral moraine (Tables 1 and 3). Collectively, our data demonstrate that Tiedemann Glacier achieved its maximum Holocene limit at about 2.7 ka.

Additional maximum limiting ages for late Neoglacial expansion of Tiedemann Glacier are 1.35–1.08 and 0.5–0.0 ka (Table 1). The 0.5–0.0 ka age range is a maximum limiting age for the uppermost exposed till in the moraine.

4.2. Regional signature of the Tiedemann Advance

Since Porter and Denton's (1967) report that alpine glaciers advanced at about 2.7 ka, additional studies have since confirmed the widespread nature of this advance in western North America. Ryder and Thomson's (1986) defined this event as the Tiedemann Advance, and the event has been subsequently recognized at other places in the British Columbia Coast Mountains (Desloges and Ryder, 1990; Clague and Mathews, 1992; Reyes and Clague, 2004; Jackson et al., 2008; Koch et al., 2007; Osborn et al., 2007; Koehler and Smith, 2011; Coulthard et al., 2013; Osborn et al., 2013); at Mount Baker (Osborn et al., 2012); the Saint Elias Mountains in Yukon Territory (Denton and Karlén, 1973, 1977); the Rocky Mountains and interior ranges of British Columbia (Osborn, 1986; Osborn and Karlstrom, 1989; Luckman et al., 1993; Luckman, 1995, 2006; Osborn et al., 2001; Wood and Smith, 2004); and Alaska (Calkin, 1988; Calkin et al., 2001; Badding et al., 2012).

What sets the Tiedemann site apart from most of the North American sites mentioned above, however, is the extent of the advance. Tiedemann Glacier at 2.7 ka advanced 1.8 km beyond its Little Ice Age limit. To our knowledge, the only two cases where glaciers can be shown through numerical dating or tephrochronology to have achieved Holocene positions more extensive than those of the Little Ice Age are in the Brooks Range in Alaska (Badding et al., 2012) and the Three Sister's volcanoes in Oregon (Marcott et al., 2009). In both cases, however, Neoglacial advances deposited moraines that were only 100 m beyond those ascribed to the Little Ice Age.

4.3. Surface debris and the magnitude of the Tiedemann Advance

The behavior of a glacier is controlled by both climate and the rate of debris added to its surface. Today, Tiedemann Glacier is heavily debris-covered, and dramatic thinning over the past 60 years has allowed debris delivered both by mass wasting of the lateral moraines and that emerging from the ice to be concentrated on its surface. This debris cover slowed the observed thinning rates for the glacier during the past 60 years (Tennant et al., 2012), but the strongly negative mass balance over this period of time compensated for the insulating effect of the debris cover.

Table 3
^{10}Be dates and external uncertainties using the various scaling methods provided by the CRONUS-Earth online calculator version 2.2 and the northeastern North American production rate (Balco et al., 2008, 2009).

Sample no.	Desilets et al. (2006)		Dunai (2001)		Lifton et al. (2005)		Time-dependent (Lal, 1991/Stone, 2000)	
	Exposure age (yr)	External uncertainty (yr)	Exposure age (yr)	External uncertainty (yr)	Exposure age (yr)	External uncertainty (yr)	Exposure age (yr)	External uncertainty (yr)
TGO-MW-01	2759	280	2794	284	2685	272	2758	279
TGO-MW-02	3305	310	3364	316	3231	303	3286	308
TGO-MW-03	2430	289	2448	291	2363	281	2443	291
TGO-MW-07	*66,349*	*33,440*	*66,355*	*33,443*	*64,047*	*32,261*	*67,339*	*33,945*
TGO-MW-08	2722	829	2755	839	2649	807	2723	829
TGO-MW-09	2624	336	2652	339	2552	326	2630	336
	Median age (ka)[1]	**iqr**[2]	**median**	**iqr**	**median**	**iqr**	**median**	**iqr**
	2.69	**0.52**	**2.72**	**0.54**	**2.71**	**0.52**	**2.69**	**0.50**

[1] Median age reported as kilo calendar age (AD1950 = 0.0 ka) to facilitate comparison with reported ^{14}C ages.
[2] Inter-quartile range.

Empirical and modeling studies suggest that a sudden introduction of debris to a glacier surface can cause the glacier to advance (Gardner and Hewitt, 1990; Shulmeister et al., 2009; Vacco et al., 2010; Shugar et al., 2012). A landslide is one way of delivering large quantities of debris to a glacier surface. In such a situation, the glacier may advance due to some combination of elevated shear stress imparted by the weight of the debris and decreased surface melt below the thick cover of debris.

Our debris advection model suggests that the sudden introduction of debris to the surface of Tiedemann Glacier could cause the glacier to advance. Our results suggest that after the initial introduction of the debris, the glacier would begin to advance after several decades and that it would achieve its maximum extent one to two centuries later. Both the simulated extent of the glacier and the thickness change agree with the geologic evidence preserved in the moraine record when our simulations involve a moderate to large debris volume (10×10^6 m^3) initially distributed near the top of the ablation zone.

We hypothesize that one or more rock avalanches delivered large amounts of debris to the ablation zone of Tiedemann Glacier shortly before 2.7 ka. Our hypothesis is consistent with simulations using our coupled, debris advection–glaciation model, which shows that even moderate-size rock avalanches could lead to a thickening and advance of the glacier comparable to that achieved during the advance at 2.7 ka.

Moderate to large rock avalanches are common in the glacierized mountains of western North America (McSaveney, 1978; Geertsema et al., 2006; Jibson et al., 2006; Shugar and Clague, 2011). In 1997, for example, a ca. 3×10^6 m^3 rock avalanche from Mount Munday, a peak adjacent to Tiedemann Glacier, traveled 4.5 km down Corridor Glacier and covered it with debris (Evans and Clague, 1998).

A moderate or large earthquake is one possible trigger for one or more large rock avalanches onto Tiedemann Glacier. The moment magnitude ($\mathbf{M_w}$) 7.9 Denali earthquake in 2002, for example, triggered thousands of rockslides and rock avalanches in the Alaska Range, many of which ran across glaciers (Jibson et al., 2006). Great earthquakes ($\mathbf{M_w} > 8$) occur at the Cascadia subduction zone, the convergent plate boundary that includes the coastal area of southwest British Columbia (Clague, 1997; Atwater et al., 2004). These earthquakes have an average recurrence of about 500 years; one of them occurred at 3.14–2.94 ka (Atwater et al., 2004). If this great earthquake triggered one or more rock avalanches that ran out onto Tiedemann Glacier, our modeling results indicate that the glacier would continue to advance for another 200 years.

Another explanation to account for the unusual behavior of Tiedemann Glacier at 2.7 ka is that it surged. There is no evidence, however, that Tiedemann Glacier, or for that matter any other glacier in the southern Coast Mountains, has surged during historic time.

Our model provides insight into the long-term response of Tiedemann Glacier following the sudden introduction of surface debris, but our results are constrained by simplifying assumptions that were required for our experiment. As described in the methods section, we do not take basal sliding into account because we lack field data required to calibrate a realistic sliding law for the glacier. The inclusion of sliding would probably decrease the response time of the glacier to an input of debris, but by exactly how much is uncertain. Another limitation is the way in which surface debris is delivered to the glacier. Our approach simplifies the introduction of the debris to the glacier and distributes this debris as a uniform debris layer. In reality, debris thickness across a glacier surface is rarely uniform. In order to simplify our experiment, we also considered the case where surface debris was instantaneously added to Tiedemann Glacier once it had reached equilibrium conditions with our prescribed mass balance forcing.

As many glaciers throughout western North America were expanding at about 2.7 ka, it is conceivable that Tiedemann Glacier was likewise advancing during this time. The sudden introduction of surface debris would thus amplify the glacier's response to an increase in surface mass balance. Finally, we estimated melt beneath surface debris on Tiedemann Glacier (Eq. (4)), which is based on empirical measurements made for other glaciers (Nicholson and Benn, 2006). Since we lack any empirical date with which to verify Eq. (4), its applicability to Tiedemann Glacier is uncertain. We stress again, however, that our modeling study was performed simply to test the hypothesis that one or more rock avalanches could cause an advance of the magnitude of the Tiedemann Advance at its type locality.

Our study is not the first to examine changes in glaciers following the sudden input of surface debris. Vacco et al. (2010) examined whether rock avalanches onto Frank Josef Glacier, New Zealand, could explain the Waiho Loop, a Younger Dryas-age end moraine that fronts the glacier. Their glacier flowline model produced hummocky terrain inside the Waiho Loop that formed when the debris-covered ice became decoupled from the active ice front and downwasted. Because no such hummocky terrain exists between the Waiho Loop and the present margin of the glacier, the authors concluded that a rock-avalanche origin for the moraine is unlikely. In the case of our study, however, we cannot use topographic features to guide our interpretation because the later advances of the Little Ice Age destroyed or covered any such landforms.

5. Conclusions

The history of Tiedemann Glacier is more complex than originally reported. Our data indicate that the glacier repeatedly advanced during the past six thousand years and that even during the Tiedemann Advance, it fluctuated markedly on decade or century timescales. Unlike the vast majority of glaciers throughout western North America, Tiedemann Glacier reached its maximum Holocene limit at about 2.7 ka. Our modeling results support the hypothesis that one or more rock avalanches caused the glacier to significantly thicken and advance.

Acknowledgements

We thank Whitesaddle Air Services for logistical support to the field site, the King family for the accommodation and hospitality, and E.J. Brook and J.D. Shakun for laboratory assistance. Funding for this research was provided by the Natural Sciences and Engineering Research Council of Canada (Discovery Grants of Clarke, Clague, Menounos, and Osborn), the Canadian Foundation for Climate and Atmospheric Sciences (Western Canadian Cryospheric Network), a Geological Society of America graduate student research grant (Marcott), a National Science Foundation (NSF) doctoral dissertation grant (Marcott), the Oregon State University R.W. Chambers undergraduate research scholarship (Novak), and a NSF grant (Clark) through the Division of Earth Sciences. Finally, we thank two anonymous reviewers for their reviews that substantially improved the quality of our paper.

References

Arsenault, T.A., Clague, J.J., Mathewes, R.W., 2007. Late Holocene vegetation and climate change at Moraine Bog, Tiedemann Glacier, southern Coast Mountains, British Columbia. Can. J. Earth Sci. 44, 707–719.

Atwater, B.F., Tuttle, M.P., Schweig, E.S., Rubin, C.M., Yamaguchi, D.K., Hemphill-Haley, E., 2004. Earthquake recurrence inferred from paleoseismology. Dev. Quat. Sci. 1, 331–350.

Badding, M.E., Briner, J.P., Kaufman, D.S., 2012. ^{10}Be ages of late Pleistocene deglaciation and Neoglaciation in the north–central Brooks Range, Arctic Alaska. J. Quat. Sci., http://dx.doi.org/10.1002/jqs.2596.

Balco, G., Brinder, J., Finkel, R.C., Rayburn, J.A., Ridge, J.C., Schaefer, J.M., 2009. Regional beryllium-10 production rate calibration for late-glacial northeastern North America. Quat. Geochronol. 4, 93–107.

Balco, G., Stone, J.O., Lifton, N.A., Dunai, T.J., 2008. A complete and easily accessible means of calculating surface exposure ages or erosion rates from ^{10}Be and ^{26}Al measurements. Quat. Geochronol. 3, 174–195.

British Columbia Ministry of Environment, Land and Parks, 1992. British Columbia Specifications and Guidelines for Geomatics, Release 2.0, Victoria, BC.

Calkin, P.E., 1988. Holocene glaciation of Alaska (and adjoining Yukon Territory, Canada). Quat. Sci. Rev. 7, 159–184.

Calkin, P.E., Wiles, G.C., Barclay, D.J., 2001. Holocene coastal glaciation of Alaska. Quat. Sci. Rev. 20, 449–461, http://dx.doi.org/10.1016/S0277-3791(00)00105-0.

Clague, J.J., 1997. Evidence for large earthquakes at the Cascadia subduction zone. Rev. Geophys. 35, 439–460.

Clague, J.J., Mathews, W.H., 1992. The sedimentary record and Neoglacial history of Tide Lake, northwestern British Columbia. Can. J. Earth Sci. 29, 2383–2396.

Clarke, G.K.C., Anslow, F.S., Jarosch, A.H., Radić, V., Menounos, B., Bolch, T., Berthier, E., 2013. Ice volume and subglacial topography for western Canadian glaciers from mass balance fields, thinning rates, and a bed stress model. J. Climate 26, 4282–4303, http://dx.doi.org/10.1175/JCLI-D-12-00513.1.

Coulthard, B., Smith, D.J., Lacourse, T., 2013. Dendroglaciological investigations of mid- to late-Holocene glacial activity in the Mt. Waddington area, British Columbia Coast Mountains, Canada. Holocene 23, 129–139.

Davis, P.T., Menounos, B., Osborn, G., 2009. Holocene and latest Pleistocene glacier fluctuations: A global perspective. Quat. Sci. Rev. 28, 2021–2033.

Denton, G.H., Karlen, W., 1973. Holocene climatic variations; their pattern and possible cause. Quat. Res. 3, 155–205.

Denton, G.H., Karlén, W., 1977. Holocene glacial and treeline variations in the White River valley and Skolai Pass, Alaska and Yukon Territory. Quat. Res. 7, 63–111.

Desilets, D., Zreda, M.G., Prabu, T., 2006. The energy dependence of cosmogenic nuclide scaling models: New measurements at low latitudes. Earth Planet. Sci. Lett. 246, 265–276.

Desloges, J.R., Ryder, J.M., 1990. Neoglacial history of the Coast Mountains near Bella Coola, British Columbia. Can. J. Earth Sci. 27, 281–290.

Dunai, T.J., 2001. Influence of secular variation of the magnetic field on production rates of in situ produced cosmogenic nuclides. Earth Planet. Sci. Lett. 193, 197–212.

Evans, S.G., Clague, J.J., 1998. Rock avalanche from Mount Munday, Waddington Range, British Columbia, Canada. Landslide News 11, 23–25.

Fulton, R.J., 1971. Radiocarbon Geochronology of Southern British Columbia. Geological Survey of Canada, Paper 71-37.

Gardner, J.S., Hewitt, K., 1990. A surge of Bualtar Glacier, Karakoram Range, Pakistan: A possible landslide trigger. J. Glaciol. 36, 159–162.

Geertsema, M., Clague, J.J., Schwab, J.W., Evans, S.G., 2006. An overview of recent large catastrophic landslides in northern British Columbia, Canada. Eng. Geol. 83, 120–143.

Goehring, B.M., 2006. ^{10}Be exposure ages of erratic boulders in Southern Norway and implications for the history of the Fennoscandian Ice Sheet. M.Sc. thesis. Oregon State University, Corvallis, OR.

Hindmarsh, R.C.A., 2001. Notes on basic glaciological computational methods and algorithms. In: Straughan, B., Greve, R., Ehrentraut, H., Wang, Y. (Eds.), Continuum Mechanics and Applications in Geophysics and the Environment. Springer, Berlin, pp. 222–249.

Jackson, S.I., Laxton, S.C., Smith, D.J., 2008. Dendroglaciological evidence for Holocene glacial advances in the Todd Icefield area, northern British Columbia Coast Mountains. Can. J. Earth Sci. 45, 83–98.

Jarosch, A.H., Anslow, F.S., Clarke, G.K.C., 2012a. High resolution precipitation and temperature downscaling for glacier models. Clim. Dyn. 38, 391–409.

Jarosch, A.H., Schoof, C.G., Anslow, F.A., 2012b. Numerical mass conservation issues in shallow ice models of mountain glaciers: The use of flux limiters and a benchmark. Cryosphere Discuss. 6, 4037–4070, http://dx.doi.org/10.5194/tcd-6-4037-2012.

Jibson, R.W., Harp, E.L., Shulz, W., Keefer, D.K., 2006. Large rock avalanches triggered by the M 7.9 Denali Fault, Alaska, earthquake of 3 November 2002. Eng. Geol. 83, 144–160.

Kessler, M.A., Anderson, R.S., Stock, G.M., 2006. Modeling topographic and climatic control of east–west asymmetry in Sierra Nevada glacier length during the Last Glacial Maximum. J. Geophys. Res. 111, F02002, http://dx.doi.org/10.1029/2005JF000365.

Koch, J., Osborn, G.D., Clague, J.J., 2007. Pre-'Little Ice Age' glacier fluctuations in Garibaldi Provincial Park, Coast Mountains, British Columbia, Canada. Holocene 17, 1069–1078.

Koehler, L., Smith, D.J., 2011. Late-Holocene glacial activity in Manatee Valley, southern Coast Mountains, British Columbia, Canada. Can. J. Earth Sci. 48, 603–618.

Lal, D., 1991. Cosmic ray labeling of erosion surfaces: In situ nuclide production rates and erosion models. Earth Planet. Sci. Lett. 104, 424–439.

Le Meur, E., Vincent, C., 2003. A two-dimensional shallow ice-flow model of Glacier de Saint-Sorlin, France. J. Glaciol. 49, 527–538.

LeVeque, R.J., 2002. Finite Volume Methods for Hyperbolic Problems. Cambridge University Press, Cambridge, UK.

Licciardi, J.M., 2000. Alpine glacier and pluvial lake records of late Pleistocene climate variability in the Western United States. Ph.D. thesis. Oregon State University, Corvallis, OR.
Lifton, N.A., Bieber, J.W., Clem, J.M., Duldig, M.L., Evenson, P., Humble, J.E., Pyle, R., 2005. Addressing solar modulation and long-term uncertainties in scaling secondary cosmic rays for in situ cosmogenic nuclide applications. Earth Planet. Sci. Lett. 239, 140–161.
Luckman, B.H., 1995. Calendar-dated, early Little Ice Age glacier advance at Robson Glacier, British Columbia, Canada. Holocene 5, 149–159.
Luckman, B.H., 2006. The Neoglacial history of Peyto Glacier. In: Demuth, M.N., Munro, D.S., Young, G.J. (Eds.), Peyto Glacier: One Century of Science. In: National Hydrology Research Institute Science Report, vol. 8, pp. 25–57.
Luckman, B.H., Holdsworth, G., Osborn, G., 1993. Neoglacial glacier fluctuations in the Canadian Rockies. Quat. Res. 39, 144–153.
Marcott, S.A., Fountain, A.G., O'Connor, J.E., Sniffen, P.J., Dethier, D.P., 2009. A latest Pleistocene and Holocene glacial history and paleoclimate reconstruction at Three Sisters and Broken Top volcanoes, Oregon, USA. Quat. Res. 71, 181–189.
Marcott, S.A., Shakun, J.D., Clark, P.U., Mix, A.C., 2013. A reconstruction of regional and global temperature for the last 11,300 years. Science 339, 1198–1201, http://dx.doi.org/10.1126/science.1228026.
McSaveney, M.J., 1978. Sherman Glacier rock avalanche, Alaska, USA. In: Voight, B. (Ed.), Rockslides and Avalanches, 1, Natural Phenomena. In: Developments in Geotechnical Engineering, vol. 14a. Elsevier Scientific, pp. 197–258.
Meier, M.F., 1962. The kinematic wave on Nisqually Glacier, Washington. J. Geophys. Res. 67, 886.
Menounos, B., Osborn, G., Clague, J.J., Luckman, B.H., 2009. Latest Pleistocene and Holocene glacier fluctuations in western Canada. Quat. Sci. Rev. 28, 2049–2074, http://dx.doi.org/10.1016/j.quascirev.2008.10.018.
Nicholson, L., Benn, D., 2006. Calculating ice melt beneath a debris layer using meteorological data. J. Glaciol. 52, 463–470.
Nishiizumi, K., Imamura, M., Caffee, M.W., Southon, J.R., Finkel, R.C., McAnich, J., 2007. Absolute calibration of ^{10}Be AMS standards. Nucl. Instrum. Methods Phys. Res. B 258, 403–413.
Osborn, G.D., 1986. Lateral moraine stratigraphy and Neoglacial history of Bugaboo Glacier, British Columbia. Quat. Res. 26, 171–178.
Osborn, G., Karlstrom, E.T., 1989. Holocene moraine and paleosol stratigraphy, Bugaboo Glacier, British Columbia. Boreas 18, 311–322.
Osborn, G.D., Luckman, B.H., 1988. Holocene glacier fluctuations in the Canadian Cordillera (Alberta and British Columbia). Quat. Sci. Rev. 7, 115–128.
Osborn, G., Menounos, B., Koch, J., Clague, J.J., Vallis, V., 2007. Multi-proxy record of Holocene glacial history of the Spearhead and Fitzsimmons ranges, southern Coast Mountains, British Columbia. Quat. Sci. Rev. 26, 479–493.
Osborn, G., Haspel, R., Spooner, I., 2013. Late-Holocene fluctuations of the Bear River Glacier, northern Coast Ranges of British Columbia, Canada. Holocene, http://dx.doi.org/10.1177/0959683612463093.
Osborn, G.D., Menounos, B., Ryane, C., Riedel, J., Clague, J.J., Koch, J., Clark, D., Scott, K., Davis, P.T., 2012. Latest Pleistocene and Holocene record glacier fluctuations on Mt. Baker, Washington, USA. Quat. Sci. Rev. 49, 33–51.
Osborn, G.D., Robinson, B.J., Luckman, B.H., 2001. Holocene and latest Pleistocene fluctuations of Stutfield Glacier, Canadian Rockies. Can. J. Earth Sci. 38, 1141–1155.
Plummer, M.A., Phillips, F.M., 2003. A 2-D numerical model of snow/ice energy balance and ice flow for paleoclimatic interpretation of glacial geomorphic features. Quat. Sci. Rev. 22, 1389–1406.
Porter, S.C., Denton, G.H., 1967. Chronology of Neoglaciation in the North American Cordillera. Am. J. Sci. 265, 177–210.
Reyes, A.V., Clague, J.J., 2004. Stratigraphic evidence for multiple Holocene advances of Lillooet Glacier, southern Coast Mountains, British Columbia. Can. J. Earth Sci. 41, 903–918.
Rinterknecht, V.R., 2004. Cosmogenic ^{10}Be chronology for the last deglaciation of the southern Scandinavian Ice Sheet. Ph.D. thesis. Oregon State University, Corvallis, OR.
Ryder, J.M., Thomson, B., 1986. Neoglaciation in the southern Coast Mountains of British Columbia: Chronology prior to the late Neoglacial maximum. Can. J. Earth Sci. 23, 273–287.
Shugar, D.H., Clague, J.J., 2011. The sedimentology and geomorphology of rock avalanche deposits on glaciers. Sedimentology 58, 1762–1783, http://dx.doi.org/10.1111/j.1365-3091.2011.01238.
Shugar, D.H., Rabus, B.T., Clague, J.J., Capps, D.M., 2012. The response of Black Rapids Glacier, Alaska, to the Denali earthquake rock avalanches. J. Geophys. Res. 117, F01006, http://dx.doi.org/10.1029/2011JF002011.
Shulmeister, J., Davies, T.R., Evans, D.J.A., Hyatt, O.M., Tovar, T.S., 2009. Catastrophic landslides, glacier behaviour and moraine formation — A view from an active plate margin. Quat. Sci. Rev. 28, 1085–1096, http://dx.doi.org/10.1016/j.quascirev.2008.11.015.
Stone, J.O., 2000. Air pressure and cosmogenic isotope production. J. Geophys. Res. 105, 23,753–23,759.
Stuiver, M., Reimer, P.J., Reimer, R.W., 2005. Calib 5.01. http://calib.qub.ac.uk/calib/.
Tennant, C., Menounos, B., Ainslie, B., Shea, J., Jackson, P., 2012. Comparison of modeled and geodetically-derived glacier mass balance for Tiedemann and Klinaklini glaciers, southern Coast Mountains, British Columbia, Canada. Glob. Planet. Change 82–83, 74–85.
Vacco, D.A., Alley, R.B., Pollard, D., 2010. Glacier advance and stagnation caused by rock avalanches. Earth Planet. Sci. Lett. 240, 123–130.
Wood, C., Smith, D.J., 2004. Dendroglaciological evidence for a Neoglacial advance of the Saskatchewan Glacier, Banff National Park, Canadian Rocky Mountains. Tree-Ring Res. 60, 59–65.
Yde, J.C., Paasche, Ø., 2010. Reconstructing climate change: Not all glaciers suitable. Eos Trans. AGU 91, 189–190, http://dx.doi.org/10.1029/2010EO210001.